Journal of Radioanalytical and Nuclear Chemistry (2019) 321:733–745
https://doi.org/10.1007/s10967-019-06636-0

Investigation of U(VI), Th(IV), and Eu(III) ions' sorption behavior onto silica gel modified with anhydride

Peizhuo Hu[1] · Yu Nan[1] · Wenya Tai[1] · Qiang Shan[1] · Yi Zhong[1] · Zhiwei Lei[1] · Tonghuan Liu[1] · Suwen Chen[1] · Lijuan Qian[1]

Received: 29 April 2019 / Published online: 4 July 2019

Abstract
Modification of silica gel by butanedioic anhydride (SiO_2–BDAH) results in efficient adsorbents for removal of U(VI), Th(IV), and Eu(III) from aqueous solutions. SiO_2–BDAH was characterized by Fourier Transform infrared spectroscopy, elemental analysis, N_2 adsorption–desorption isotherms, thermogravimetic analysis, and potentiometric titration. The effect of contact time, pH, and initial concentration of radioactive solutions and temperature on the adsorption capacity of the sorbent was investigated. The sorption equilibrium times of U(VI), Th(IV), and Eu(III) onto SiO_2–BDAH were 1.5, 2, and about 10 h. The sorption percentages of U(VI), Th(IV), and Eu(III) increased with increased pH from 1 to 5. The sorption process of U(VI), Th(IV), and Eu(III) can be described by the Langmuir model, with sorption capacities of 5.10×10^{-5}, 5.06×10^{-5}, and 3.44×10^{-5} mol/L, respectively. The enthalpy and entropy changes were all positive, whereas the free energy changes were negative. This study indicated that SiO_2–BDAH can remove U(VI) and Th(IV) at the same time in the presence of multiple ions from waste water quickly.

Keywords Uranyl · Thorium · Europium · Silica gel · Anhydride · Sorption

Introduction

Primordial actinides (Th, U) and their associated mineral rare-earth elements have wide-ranging practical applications [1, 2]. Uranium has extensive applications in the nuclear power industry, while ^{232}Th is a potential nuclear fuel because of its good fertile characteristic [3]. Rare-earth elements and their compounds have a wide range of applications especially in metallurgy, ceramic industry, and nuclear fuel control [4]. However, these elements exhibit serious threat to the environment, because most processes and activities are related to nuclear fuel cycles including mining and process and spent nuclear reprocessing [5]. Actinide and lanthanide elements are heavy metals with chemical toxicity and radioactivity, which causes progressive or irreversible renal injury, and their compounds are potential carcinogens [3, 5, 6]. Thus, the removal of actinide and lanthanide ions from contaminated waters are attractive for the environment.

✉ Lijuan Qian
qianlj@lzu.edu.cn

[1] School of Nuclear Science and Technology, Lanzhou University, Lanzhou 73000, People's Republic of China

A series of approach can be applied to metal ion removal from waters, based on precipitation, liquid–liquid extraction methods, exchange resins, membrane filtration, and adsorption [8, 9]. Adsorption separation is an extraction and concentration technique that is developed in the recent years based on the sorbent, which is the best and effective candidate for metal ion removal from aqueous solutions with moderate and low concentrations. In sorption process, it is important to select the suitable sorption material, some of them are often prepared for fixing functional organic compounds on resins, cellulose, fibers, activated carbon, sand, clay, zeolites, polymers, metal oxides, and highly dispersed silica gel [10, 11].

Silica is a good support because of its high thermal, chemical, and mechanical stability. Its surface is modified by functional groups, such as amino [12, 13], carboxyl [14], amide groups [15–17], Schiff base [18–20], and complex groups [21, 22], which have been reported for concentrating metals in environmental medium.

Amide extractants are studied in the extraction of actinides and lanthanides for the ease of synthesis, high chemical, and radiolytic stability [23, 24]. Based on these properties, amides extractants are grafted on silica gel, nanometer

silica, or porous silica to separate actinides and lanthanides [17, 25–27]. These solid-phase extraction agents form amido podans structure, owning diamide group, ether bond, and alkyl at the substrate. Trivalent lanthanides and actinides could coordinate with six oxygens from the carbonyl (coming from bisamides) and ether group providing by graft group on the surface of silica [17]. Suneesh [14] synthesized SiO_2–DGAH which modified the surface of silica gel with diglycolamic acid moieties, and forming single amide group and carboxyl at the surface of silica gel. SiO_2–DGAH could coordinate with Am(III) and Eu(III) rapidly same as bisamide structure sorbents and the adsorption equilibrium occurring within 30 min [14].

Butanedioic anhydride (BDAH) was used to modify silica gel forming the composite solid-phase extractants (SiO_2–BDAH) in this study, which it is very cheap for BDAH and silica gel are all simple industry material. SiO_2–BDAH contains single amide group and carboxyl groups when BDAH bind with silane coupling agent 3-aminopropyltriethoxysilane (APTS) on the surface of silica. In this study, SiO_2–BDAH was synthesized and characterized, and SiO_2–DGAH was as an analogue. The effects of various parameters such as duration of equilibrations, pH, initial metal ion concentration, temperature of U(VI), Th(IV), and Eu(III) sorption on SiO_2–BDAH were studied. The objective of this study was to remove lanthanide and actinide ions from radioactive wastewater on silica functionalized with carboxylic and amide groups in static system, based on various experimental parameters.

Experimental

Materials

All chemicals and reagents used in the study were of analytical grade, including silica gel (mesh size 100) (Qingdao Hailang silica gel desiccant Co., LTD, China), APTS (Aladdin). BDAH, DGAH (diglycolamic acid) (Sinopharm Chemical Reagent Co., LTD, China). U(VI) and Th(IV) stock solutions were prepared from $UO_2(NO_3)_2{\cdot}6H_2O$ and $Th(NO_3)_4{\cdot}4H_2O$ (China), respectively. The Eu(III) stock solution was prepared by dissolving Eu_2O_3 (99.99%) in hydrochloric acid (HCl). $^{152+154}$Eu(III) radiotracer was obtained from the China Institute of Atomic Energy.

Synthesis of new sorbent

Silica gel was activated according to Ref. [28] with slight modifications, where silica gel (100 mesh, 50 g) was refluxed with 50 mL HCl (18%) solution for 24 h, then filtered and repeatedly washed with an appropriate amount of deionized water until the filtrate was neutral. The activated silica was dried in an oven at 60 °C for 48 h.

A sample 15 g activated silica gel was suspended in 100 mL acetic acid (pH = 3) and added with 15 mL APTS. The mixture was refluxed under dry nitrogen atmosphere for 16 h at 85 °C, and the modified silica gel was filtered off, washed thrice with distilled water, twice with isopropanol, absolute ethyl alcohol, and dried under vacuum at 60 °C [28]. Finally, SiO_2–APTS was prepared (Fig. 1a).

A sample of 8.0 g SiO_2–APTS and 3.0 g BDAH (DGAH) were added to 100 mL of menthol. The mixture was reacted for 3 h in a reflux system at 60 °C. The solid phase was filtered, washed with ethyl acetate and absolute ethyl alcohol, and dried under vacuum at 60 °C for 24 h. It was named as SiO_2–BDAH and SiO_2–DGAH (Fig. 1b, c).

Potentiometric titration

A sample of 0.25 g SiO_2–BDAH (SiO_2–DGAH) was dispersed in 60 mL $NaNO_3$ (0.1, 0.01, and 0.001 mol/L). The suspension was stirred under argon atmosphere for 12 h. Then, standard HCl (0.05 mol/L) was added until pH ~ 3.5 was reached. The suspension was titrated with NaOH (0.05 mol/L) until pH ~ 9.5. Then, titration from pH 9 to 4 was carried out sequentially by using standard HCl for the same suspension. The incremental volume during titration was fixed at 50 µL. The pH was recorded when the variation of the potential became less than 0.5 mV/min (equivalent to about 0.01 pH units per min) or the interval was more than 10 min. The total duration of titration from pH 4 to 9 (or from 9 to 4) was at most 3 h. Blank titrations were carried out following the same method except that the incremental volume was fixed at 6 µL. The titrations were carried out in a glass vessel by using Metrohm Titrando 709 with a combined electrode (Metrohm 6.026.100). The temperature of the glass vessel was fixed at 25 °C through water circulation [29, 30].

Measurement of graft content

Graft content can be measured by Elemental Analyzer (Elementar, German), which would show the content of C, N, and H. The C/N ratio can obtain the graft content of silica gel.

Characterization

The structure of SiO_2–BDAH and SiO_2–DGAH was characterized by FT-IR and BET. FT-IR spectra were obtained by using NEXUS 670 (Nicolet, USA) in KBr pellet at room temperature. N_2 adsorption–desorption isotherms were measured at − 195.8 °C by using TriStar II 3020 V1.04(Micromeritics Instrument Corporation, USA).

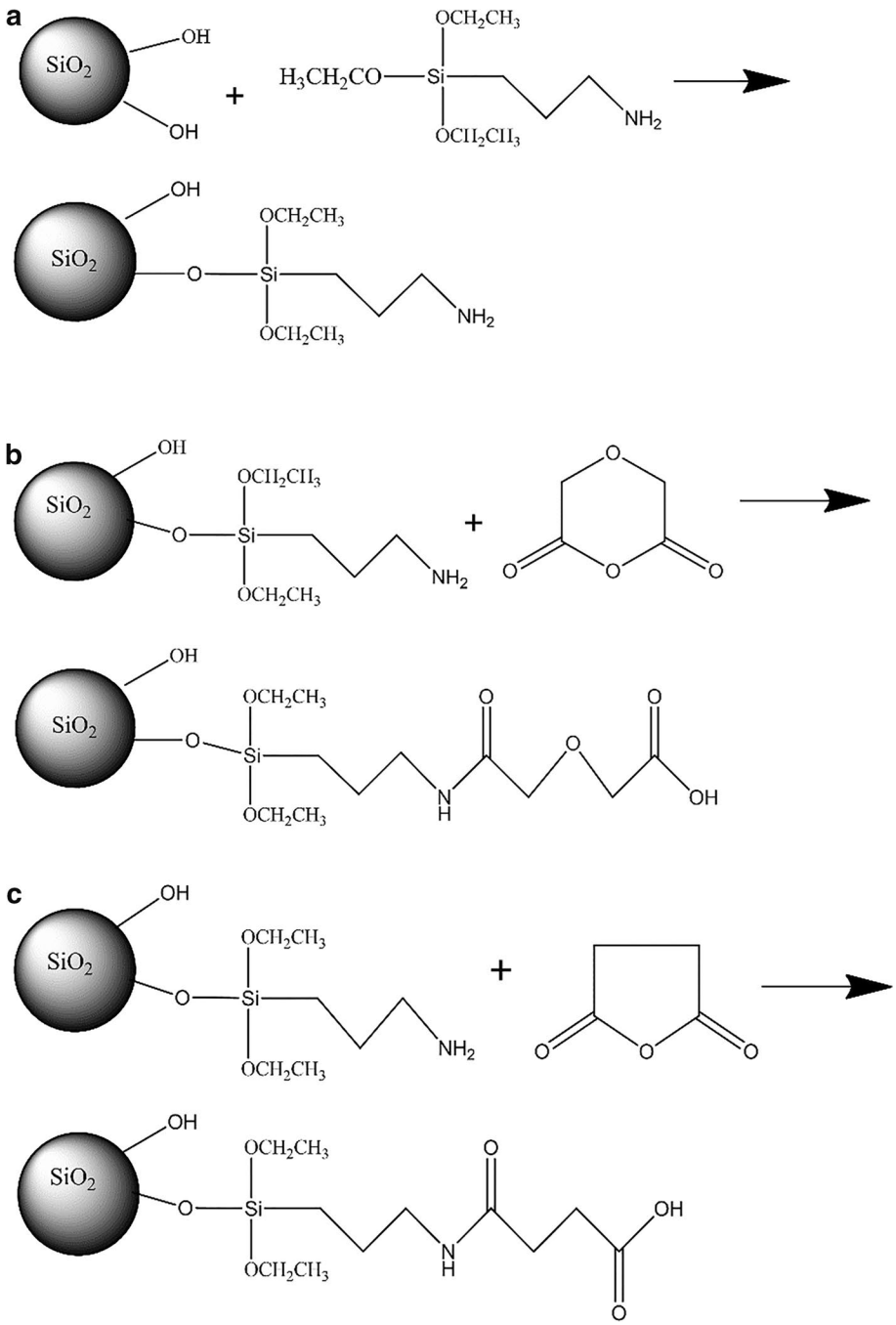

Fig. 1 Synthesis of SiO_2–APTS (**a**), SiO_2–DGAH (**b**), SiO_2–BDAH (**c**)

Thermogravimetric analysis (TGA) was determined by a LINSEIS STAPT 1600 (Linseis Corporation, Selb, Germany) in nitrogen at a heating rate of 10 10 K/min, scanning temperature were shown in the range from 25 to 900 °C.

Sorption studies of SiO_2–BDAH and SiO_2–DGAH for U(VI), Th(IV), and Eu(III)

Sorption was performed with batch technique in an aqueous solution for U(VI), Th(IV), and Eu(III) at 25 ± 2 °C. A sample of 25.0 mg SiO_2–BDAH (SiO_2–DGAH) was suspended in 10.0 mL of aqueous solution containing variable amounts of each cation in the sample shaker vessel. For these sorption measurements, different amounts of derived silica sorbent were suspended 10 mL of aqueous solution containing variable amounts of every cations, whose concentrations vary within 10–30 mg/L in an orbital shaker thermostat for 4 h (optimum condition, at room temperature, and different pH values).

After equilibrium was established, the suspension was filtered, and the amounts of metallic cations remaining in the solution were determined by spectrophotometry for U(VI) and

Th(IV) [31, 32] and liquid scintillation analyzer for Eu(III) [33]. Multiple metal ions were measured simultaneously by ICP-OES (5100, Agilent Technologies). The amount of metal ions sorbed by the sorbents was calculated as follows (1):

$$R\% = (C_0 - C)/C_0 \times 100 \quad (1)$$

where $R\%$ is the amount of metal ion sorbed onto a unit amount of the sorbent (mmol/g), and C_0 and C are the concentrations of metal ions in the initial and equilibrium concentrations of the metal ions in aqueous phase (mmol/L), respectively.

Desorption Performance Study of U(VI), Th(IV), and Eu(III)

The desorption behavior of U(VI), Th(IV), and Eu(III) on SiO_2–BDAH in relation to concentration of desorption reagent was carried out after the sorption experiment. From an economic point of view, the optimal desorption conditions were studied and the desorption percentage of U(VI), Th(IV), and Eu(III) on sorbent was calculated using the sorption amount of U(VI), Th(IV), and Eu(III) on the sorbent (C_s, mol/g) and their concentration in the solution after desorption (C_e, mol/L), as follows (2):

$$D\% = C_e/C_s \times V/m \times 100 \quad (2)$$

where m is amount of the sorbent and V is the volume of solution.

Result and discussion

Characterization of SiO_2–BDAH and SiO_2–DGAH

The prepared amide ligands were characterized through FT-IR spectroscopic method (Fig. 2). Several peaks were observed in the IR spectra of the four curves such as (1) a band assigned to Si–OH stretching frequency and flexible frequency coming from the hydrogen bond between the adsorbed water at 1634.3 and 3430 cm^{-1}; and (2) the sharp peak at 1098.3 cm^{-1} that is related to Si–O–Si group vibrations [34]. After modification with APTS (curve b), the band at 2947.7 and 2864.2 cm^{-1} were attributed to the stretching frequency of C–H for SiO_2–APTS. After modification with anhydride (curve c, d), the peak around 1647.1 and 1641.1, and 1735.3 cm^{-1} were attributed to the stretching vibration mode of the C=O (NH–CO) groups, C=O (COOH) of SiO_2–BDAH and SiO_2–DGAH, respectively, and the peak at 1418 cm^{-1} was due to the stretching vibration of C–N [35]. The results of IR spectra clearly show that SiO_2–APTS, SiO_2–BDAH, and SiO_2–DGAH were immobilized on the silica surface [36].

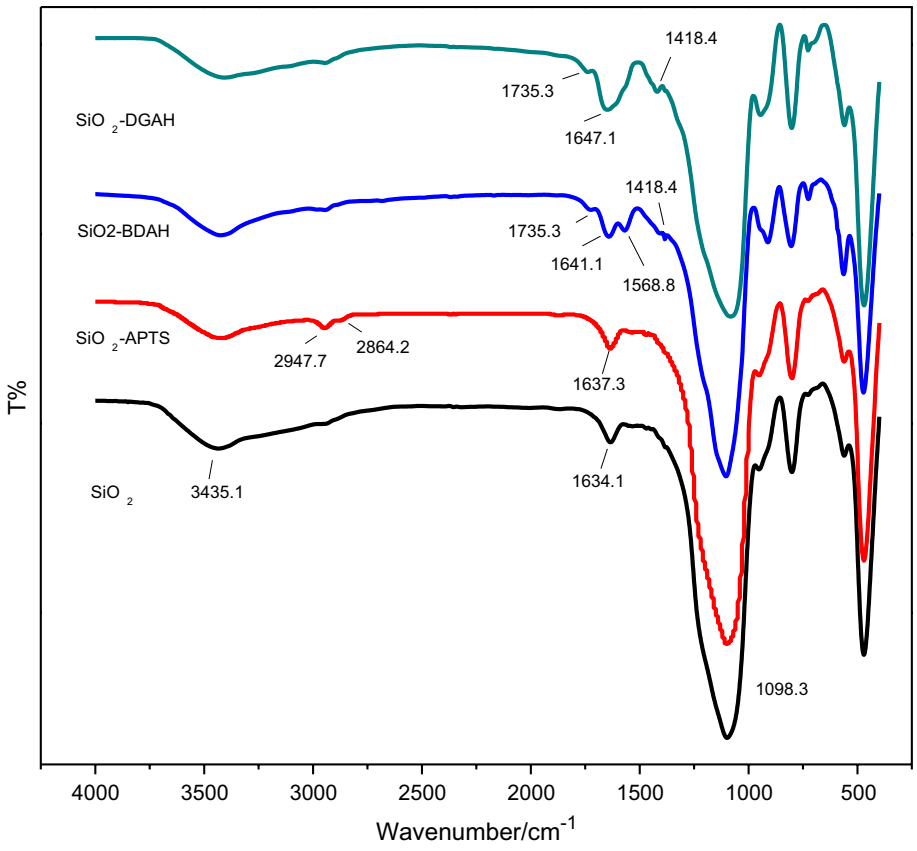

Fig. 2 FT-IR spectra of SiO_2, SiO_2–APTS, SiO_2–DGAH, and SiO_2–BDAH

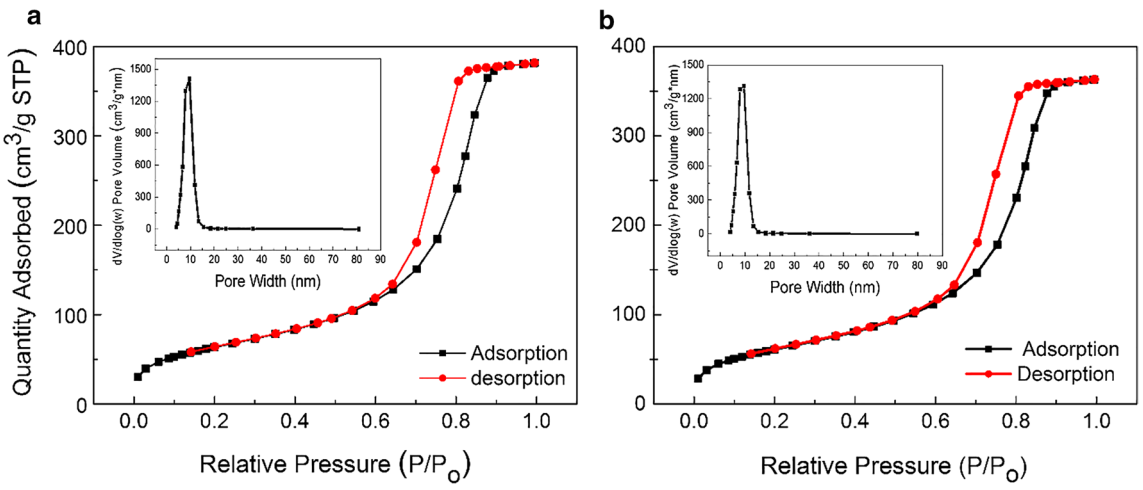

Fig. 3 N_2 adsorption–desorption isotherms measured at − 195.8 °C for SiO_2–DGAH (**a**) and SiO_2–BDAH (**b**)

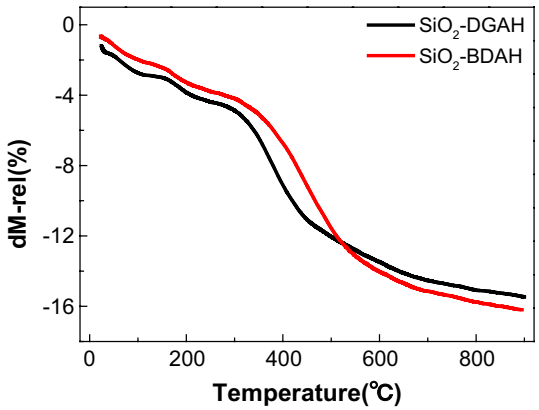

Fig. 4 TG pattern obtained for SiO_2–DGAH and SiO_2–BDAH

The nitrogen adsorption–desorption isotherms were used to characterize the microstructure of SiO_2–BDAH and SiO_2–DGAH, and the results are presented in Fig. 3a, b. The surface area is 222.92 and 230.00 m^2/g and the pore size is 10.08 and 10.27 nm for SiO_2–BDAH and SiO_2–DGAH, respectively. SiO_2–DGAH has a slightly higher surface area and pore size. From Fig. 3a, b, the effective mesoporous structure with a small number of micropores can be confirmed by the type H3 hysteresis loop on the BET curve of SiO_2–BDAH and SiO_2–DGAH according to the IUPAC classification [27, 37].

TG curves of SiO_2–BDAH and SiO_2–DGAH are shown in Fig. 4. The first weight loss of SiO_2–BDAH and SiO_2–DGAH (2.0% and 2.5%, respectively) at about 25–100 °C is related to the physisorbed water evaporation which trapped on the surface and inside of the sorbents. Then dehydration reaction occurs between the two adjacent carboxylic acid groups and leads to weight loss of SiO_2–BDAH and SiO_2–DGAH (about 4.8%) at the temperature range of 100 to 300 °C [14]. The decomposition of the organic moieties grafted on the surface of SiO_2–BDAH and SiO_2–DGAH causes to weight loss (16.1% and 15.4%, respectively) at the temperature range of 300 to 900 °C. TG curves of SiO_2–BDAH and SiO_2–DGAH has slight difference for the structure of BDAH and DGAH has tiny difference.

Table 1 The content of N, C, and H by elemental analysis

	N%	C%	H%	C%/N%
SiO_2–APTS 1	1.82	6.29	1.48	3.23
SiO_2–APTS 2	1.81	6.18	1.52	3.19
SiO_2 1	0	0.48	0.72	
SiO_2 2	0	0.35	0.66	

Elemental analysis and graft content

The percentages of C, H, and N were evaluated by elemental analysis and are presented in Table 1. For the functionalized silica gels, the percentage of C decreases with increased degree of cross-linking. The N content comes from the terminal group of APTS. The C/N value is 36/14 (2.57) and 60/14 (4.28) when APTS loses two and three ethyoxyl groups, respectively. From Table 1, the amount of N and C on SiO_2–APTS 1 and SiO_2–APTS 2 was 1.82%, 6.29% and 1.81%, 6.18%, and C %/N % is about 3.2, deducting the C amount in SiO_2. Therefore, the degree of cross-linking of SiO_2 and APTS is between 2 and 3.

Potentiometric titration

The proton excess of SiO_2–BDAH or SiO_2–DGAH (ΔQ^H, mol/g) was determined by subtracting the titration curve

of the background electrolyte solution (blank) from that of SiO_2–BDAH or SiO_2–DGAH suspension [29, 30]

$$(C_A - C_B)_{susp} = [H^+] - [OH^-] + \Delta Q_{solid} + \Delta Q_{blank} \quad (3)$$

$$(C_A - C_B)_{blank} = [H^+] - [OH^-] + \Delta Q_{blank} \quad (4)$$

$$\Delta Q^H = V/m[(C_A - C_B)_{susp} - (C_A - C_B)_{blank}] \quad (5)$$

where C_A and C_B (mol/L) are the concentrations of acid and base added, respectively, ΔQ_{blank} (mol/L) represents the consumption or release of H^+ by side-reactions, ΔQ_{solid} (mol/L) and ΔQ^H(mol/g) represent the proton excess of SiO_2–BDAH or SiO_2–DGAH in different units, respectively, V (L) is the volume of aqueous solution, and m (g) is the mass of SiO_2–BDAH or SiO_2–DGAH.

Figure 5a, b illustrates the titration results of SiO_2–DGAH and SiO_2–BDAH at three ionic strengths (0.1, 0.01, and 0.001 mol/L NaCl). The titration curve of SiO_2–DGAH and SiO_2–BDAH shows that surface charges consistently decreases with the increases of pH in different ionic strength solution and the slope of decline is not consistent. An intersection exists when the solution pH varies from low to high value at the three ionic strengths. The intersection is named as point of zero charge (PZC), and the PZC of SiO_2–BDAH and SiO_2–DGAH is about 4.25 as obtained from Fig. 5a, b. The surface charge of SiO_2–BDAH and SiO_2–DGAH is negative when pH is over 4.25 while is positive below 4.25. The ionic strength has an effect on the decline slope of surface charge. Figure 5a, b shows that the effect of ionic strength to SiO_2–BDAH is greater than that of SiO_2–DGAH, indicating that ether bond group of SiO_2–DGAH has complicate effect.

Time dependency of the sorption process

The sorption of U(VI), Th(IV), and Eu(III) onto SiO_2–BDAH and SiO_2–DGAH was studied as a function of contact time to determine the corresponding equilibrium time. The effect of contact time on the removal of U(VI), Th(IV), and Eu(III) was presented in Fig. 6a–c, and the fitting kinetic parameters of pseudo-second order was listed on Table 2. The pseudo-second order rate equation (6) was used to simulate the kinetic sorption [32, 33]:

$$\frac{t}{q_t} = \frac{1}{kq_e^2} + \frac{t}{q_e} \quad (6)$$

where k (g mg^{-1} h^{-1}) is the pseudo-second order rate constant for the sorption, q_t (mg g^{-1} of dry, mass) is the amount of U(VI), Th(IV), and Eu(III) sorbed on the surface of the adsorbent at time t (h), and q_e (mg g^{-1} of dry mass) is the equilibrium sorption capacity. The k and q_e values can be calculated from the slope and intercept.

The sorption equilibrium time of U(VI), Th(IV), and Eu(III) onto SiO_2–DGAH is 3, 2, and 2 h, respectively, which takes longer time than that of other references [14, 25, 26]. The equilibrium time of metal ions is about dozens of minutes when the concentration of metal ions is tens of micrograms per liter, which is shorter than that in this study. Shusterman [17] found that the contact time is

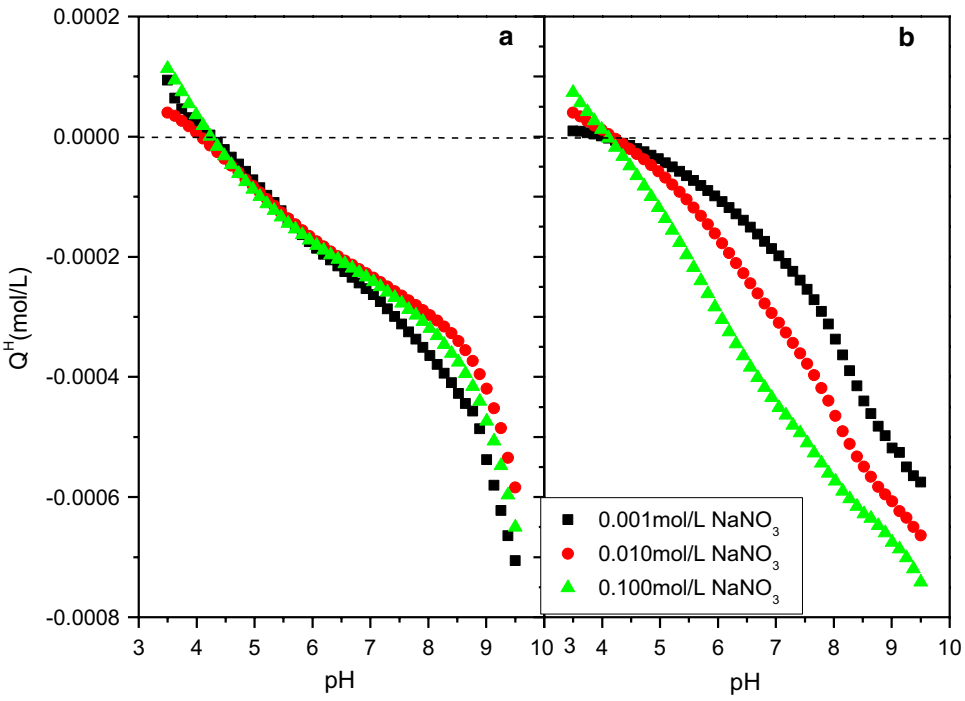

Fig. 5 Proton excess of SiO_2–DGAH (**a**) and SiO_2–BDAH (**b**) as a function of pH at three ionic strengths

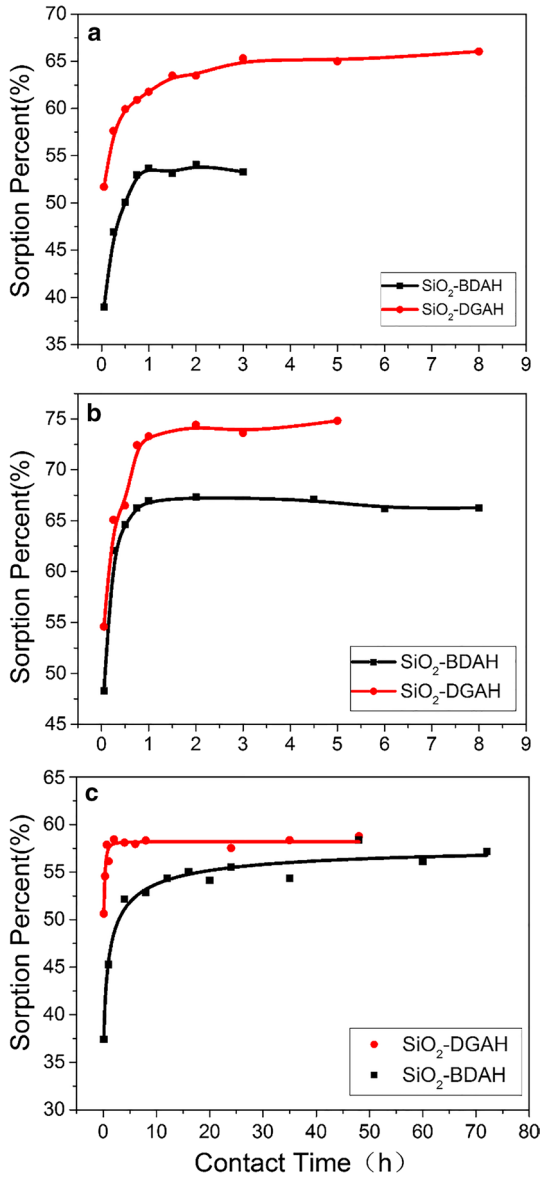

Fig. 6 Effect of time on the sorption of U(VI) (**a**), Th(IV) (**b**), and Eu(III) (**c**) onto SiO_2–DGAH and SiO_2–BDAH. **a** $C(UO_2^{2+})_0 = 1.88 \times 10^{-4}$ mol/L, $m/V = 2.5$ g/L, $C(Na^+) = 0.1$ mol/L, $T = 25 \pm 2$ °C, pH = 3.1 ± 0.1 (SiO_2–DGAH), pH = 3.0 ± 0.1 (SiO_2–BDAH). **b** $C(Th^{4+})_0 = 2.48 \times 10^{-4}$ mol/L, $m/V = 2.5$ g/L, $C(Na^+) = 0.1$ mol/L, $T = 25 \pm 2$ °C, pH = 2.5 ± 0.1. **c** $C(Eu^{3+})_0 = 2.00 \times 10^{-4}$ mol/L, $m/V = 5$ g/L, $C(Na^+) = 0.1$ mol/L, $T = 25 \pm 2$ °C, pH = 2.6 ± 0.1 (SiO_2–DGAH), pH = 3.6 ± 0.1 (SiO_2–BDAH)

about 2 h when the Eu concentration is 8 μmol/L. Hence, the equilibrium time of U(VI), Th(IV), and Eu(III) onto SiO_2–DGAH in this study is suitable for a concentration of about 2×10^{-4} mol/L. From Table 2, the sorption equilibrium time of U(VI) and Th(IV) onto SiO_2–BDAH is 1.5 and 2 h, respectively, which is almost same for SiO_2–DGAH. Moreover, the sorption equilibrium time of Eu(III) is about 10 h, which is longer than that for SiO_2–DGAH. However, the sorption percent of Eu(III) slightly varies after 5 h from Fig. 6c, and perhaps, physical diffusion results to a slow sorption process.

The experimental results can be modeled by the pseudo-second order model and fits the experimental data quite well for R^2 values of over 0.999. The q_e of U(VI), Th(IV), and Eu(III) onto SiO_2–BDAH is 4.05×10^{-5}, 6.63×10^{-5}, and 2.29×10^{-5} mol/g, respectively, which is slightly lower for SiO_2–DGAH. SiO_2–DGAH has ether bond, indicating more sorption sites than SiO_2–BDAH. The order of U(VI), Th(IV), and Eu(III) sorption amount is Th(IV) > U(VI) > Eu(III), which is the same for the two adsorbent.

Effect of pH

The sorption percentage of U(VI), Th(IV), and Eu(III) onto SiO_2–BDAH and SiO_2–DGAH as a function of pH are shown in Fig. 7a–c. The sorption of U(VI) onto SiO_2–BDAH and SiO_2–DGAH dealt a sharp increase in sorption percentage from 5 to 90% of the added U(VI) concentration between pH 2–4 at $m/V = 2.5$ g/L from Fig. 7a. The sorption amount of U(VI) onto SiO_2–DGAH is slightly higher than that of SiO_2–BDAH at pH < 3.5 but is the reverse at pH > 3.5. From Fig. 7b, the sorption edge of Th(IV) onto SiO_2–BDAH from 0 to 98% of the added Th(IV) concentration arises between pH 1.5–3 at $m/V = 2.5$ g/L. However, the sorption curve of Th(IV) onto SiO_2–DGAH has a sorption platform at 70% for pH 2.5–4. The sorption curve of Eu(III) onto SiO_2–BDAH and SiO_2–DGAH are shown on Fig. 7c. The sorption edge of Eu(III) onto SiO_2–BDAH from 0 to 98% of the added Eu(III) concentration appears between pH 2.5–4.5 at $m/V = 5.0$ g/L. From Fig. 7c, the sorption of Eu(III) onto SiO_2–DGAH has a higher increase at low pH with a weaker sorption at high pH than that onto SiO_2–BDAH. The sorption percentage of U(VI), Th(IV), and Eu(III) onto SiO_2–DGAH is higher than that onto SiO_2–BDAH at low pH, but is the reverse at

Table 2 Kinetic parameters for UO_2^{2+}, Th^{4+}, and Eu^{3+} sorption onto modified SiO_2

	SiO_2–BDAH			SiO_2–DGAH		
	U	Th	Eu	U	Th	Eu
pH	3.0 ± 0.1	2.5 ± 0.1	3.6 ± 0.1	3.1 ± 0.1	2.5 ± 0.1	2.6 ± 0.1
Equilibrium time/h	1.5	2	10	3	2	2
q_{max} ($\times 10^{-5}$ mol/g)	4.05	6.63	2.29	4.90	7.20	2.34
K (g mg^{-1} h^{-1})	4.57	11.22	4.57	3.13	14.58	3.12
R^2	0.9997	0.9995	0.9991	0.9999	0.9995	0.9999

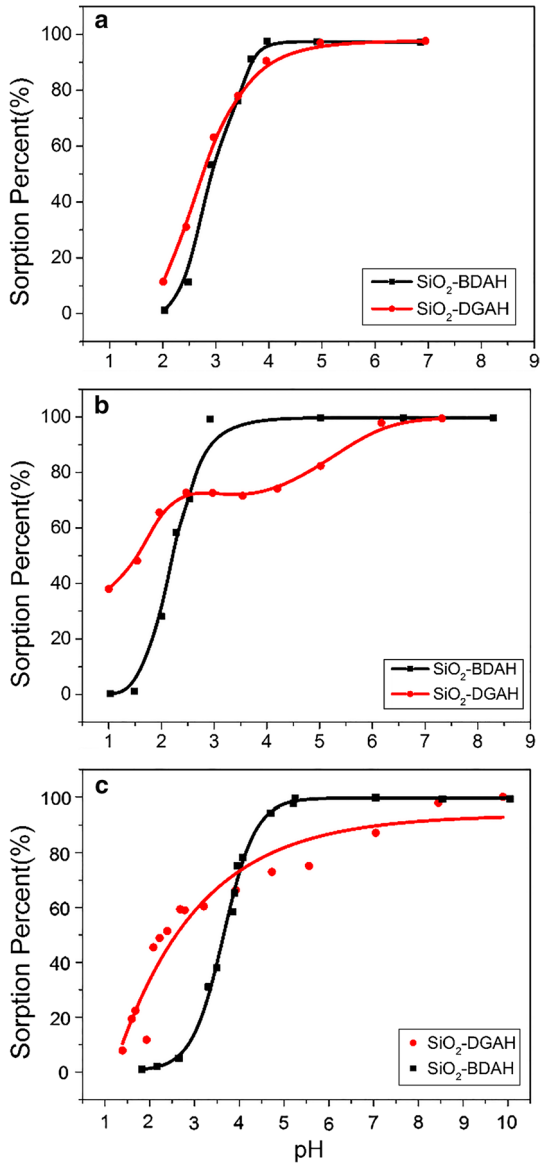

Fig. 7 Effect of pH on the sorption of U(VI) (**a**), Th(IV) (**b**), and Eu(III) (**c**) onto SiO_2–DGAH and SiO_2–BDAH. **a** $C(UO_2^{2+})_0 = 1.88 \times 10^{-4}$ mol/L, $m/V = 2.5$ g/L, $C(Na^+) = 0.1$ mol/L, $T = 25 \pm 2$ °C, $t = 3$ h (SiO_2–DGAH), $t = 2$ h (SiO_2–BDAH). **b** $C(Th^{4+})_0 = 2.48 \times 10^{-4}$ mol/L, $m/V = 2.5$ g/L, $C(Na^+) = 0.1$ mol/L, $T = 25 \pm 2$ °C, $t = 2$ h (SiO_2–DGAH), $t = 3$ h (SiO_2–BDAH). **c** $C(Eu^{3+})_0 = 2.00 \times 10^{-4}$ mol/L, $m/V = 5$ g/L, $C(Na^+) = 0.1$ mol/L, $T = 25 \pm 2$ °C, $t = 3$ h (SiO_2–DGAH), $t = 48$ h (SiO_2–BDAH)

high pH according to Fig. 7a–c. The sorption process of U(VI), Th(IV), and Eu(III) is very sensitive to pH for the sorbents of SiO_2–BDAH and SiO_2–DGAH contain acidic functional moieties (-COOH) on the surface of silica gel and cation exchange reaction could take place. However, the SiO_2–DGAH surface has an ether bond, which complicates to the metal ion sorption. From Fig. 3a, the titration curves of SiO_2–DGAH under the three ionic strengths are very intricate. Hence, it is easy to understand complicated sorption behavior the U(VI), Th(IV), and Eu(III) onto SiO_2–DGAH. In short, SiO_2–BDAH has high sorption amount and simple sorption process comparing to SiO_2–DGAH at weak acid condition.

Effect of temperature and sorption isotherm model-fitting

The sorption isotherms of U(VI) and Th(IV) at 298, 318, and 338 K and Eu(III) at 298, 308, and 318 K onto SiO_2–BDAH are shown in Fig. 8a–c. The pH values of the suspension has little variation when the sorption experiments for U(VI), Th(IV), and Eu(III) began and finished. The solution pH labelled on Fig. 8 is the value when sorption finished. The sorption isotherms of $C_e \sim q_e$ are linear according to Fig. 8a–c. The linear isotherm indicates the partitioning of the solutes from the liquid to solid surface. The Freundlich model is linear on a log–log graph and is often regarded as an empirical relationship describing the sorption of solutes from a liquid to a solid surface (see formulae 7, 8). The Langmuir model assumes no interaction between the adsorbent molecules and a monolayer sorption process (see formula 9). Generally, the Freundlich model is more suitable for large sorption percentages than the Langmuir model

$$q_e = K_F C_e^{1/n} \tag{7}$$

$$\log q_e = \log K_F + 1/n \log C_e \tag{8}$$

$$\frac{C_e}{q_e} = \frac{1}{q_{max} K_L} + \frac{C_e}{q_{max}} \tag{9}$$

where q_e is the amount of U(VI), Th(IV), and Eu(III) sorbed per mass unit of SiO_2–BDAH (mol/g), n and K_F, K_L are empirical constants, and q_{max} is the saturated amount (mmol/g). The relative parameters of the Freundlich and Langmuir model fitting for the U(VI), Th(IV), and Eu(III) sorbed onto SiO_2–BDAH are listed in Table 3. The R^2 for the Langmuir and Freundlich isotherms are over 0.92 for U(VI) and Eu(III) onto SiO_2–BDAH but is very low for Th(IV) sorption for the Freundlich isotherm. Hence, the sorption process of U(VI), Th(IV), and Eu(III) can be described by the Langmuir model, which indicates a monolayer sorption onto SiO_2–BDAH. The q_{max} of U(VI), Th(IV), and Eu(III), obtained from the Langmuir model (see Table 3) increases with increased temperature. The q_{max} at 298 K is the same as the q_e obtained from the pseudo-second order model (see Table 2). Suneesh [14] obtained the Eu(III) sorption capacity of SiO_2–DGAH of 3.2×10^{-5} mol/L at pH = 2, which is consistent with this study. Hence, SiO_2–BDAH has a good characteristic to sorb Eu(III) compared with SiO_2–DGAH and has a better sorption capacity for U(VI) and Th(IV) than Eu(III). Juère [37] found that sorption capacity to Eu(III)

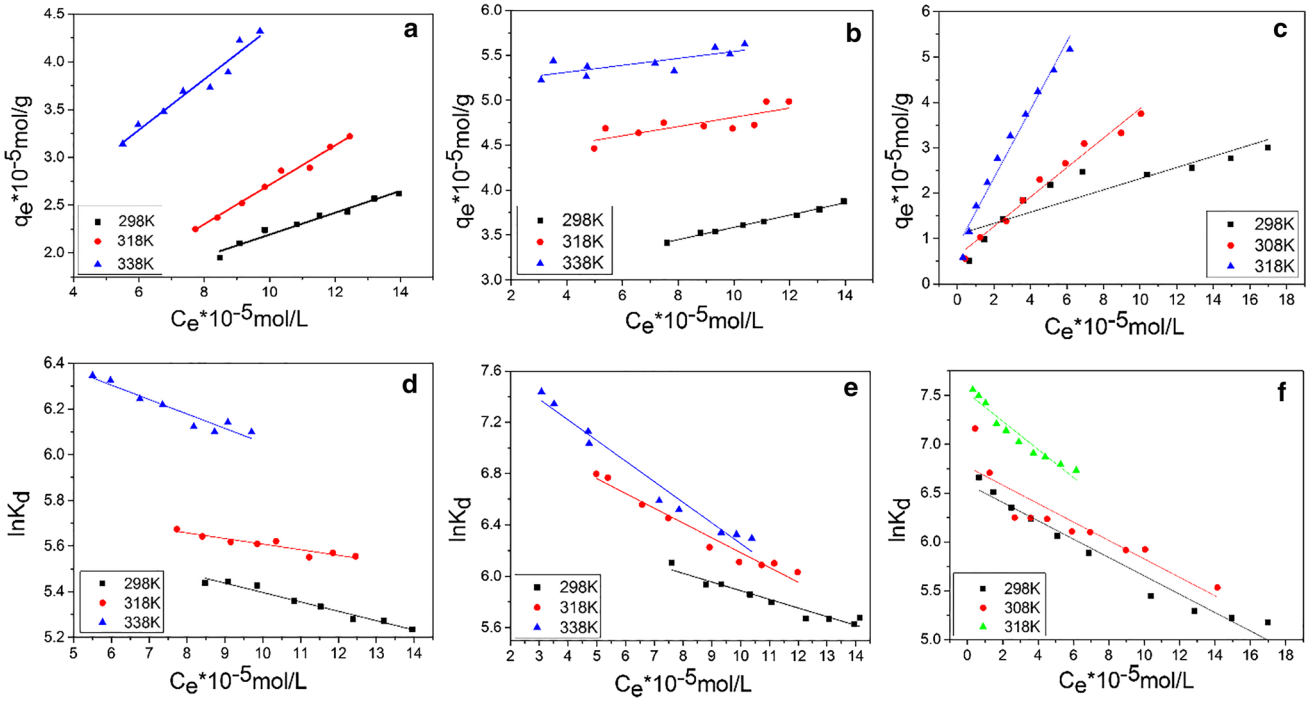

Fig. 8 Sorption isotherms of U(VI) (**a**), Th(IV) (**b**), and Eu(III) (**c**) onto SiO_2–BDAH at different temperatures and Linear fit of $\ln K_d$ versus C_e using the sorption isotherms of U(VI) (**d**), Th(IV) (**e**), and Eu(III) (**f**) on SiO_2–BDAH. **a** U(VI): $m/V = 2.5$ g/L, $C(Na^+) = 0.1$ mol/L, pH = 2.8 ± 0.1, $t = 2$ h. **b** Th(IV): $m/V = 2.5$ g/L, $C(Na^+) = 0.1$ mol/L, pH = 2.1 ± 0.1, $t = 3$ h. **c** Eu(III): $m/V = 5.0$ g/L, $C(Na^+) = 0.1$ mol/L, pH = 3.9 ± 0.1, $t = 48$ h

Table 3 Parameters evaluated using Freundlich and Langmuir isotherms for U(VI), Th(IV), and Eu(III) sorption onto SiO_2–BDAH at different temperatures

Metal ions	pH	Temperature (K)	Freundlich isotherm			Langmuir isotherm		
			$\log K_F$ [(mol/g)/(mol/L)$^{1/n}$]	n	R^2	K_L (g/L)	q_{max} (mol/g)	R^2
UO_2^{2+}	2.8 ± 0.1	298	− 2.46	1.32	0.9712	0.36	5.10×10^{-5}	0.9681
		318	− 2.26	1.81	0.9869	0.39	7.91×10^{-5}	0.879
		338	− 1.55	1.89	0.928	0.93	11.10×10^{-5}	0.9222
Th^{4+}	2.1 ± 0.1	298	− 4.24	147.06	0.0067	1.21	5.06×10^{-5}	0.9477
		318	− 4.04	14.25	0.2993	6.82	5.13×10^{-5}	0.979
		338	− 3.39	3.78	0.7615	77.52	5.48×10^{-5}	0.9926
Eu^{3+}	3.9 ± 0.1	298	− 2.6	2.01	0.9246	0.99	3.44×10^{-5}	0.9869
		308	− 2.12	1.71	0.9793	0.98	5.13×10^{-5}	0.9315
		318	− 1.30	1.42	0.9918	1.96	8.37×10^{-5}	0.9802

is about 22, 25, and 26 mg/g for DGA-functionalized mesoporous silica SBA15(80), SBA-15(130), and MCM-41, respectively, which is several times higher than our reported values. The reason could be attributed to its small pore sizes of MCM-41 and large surface area. The pore size of SiO_2–DGAH in this article is 10.1 nm, which is higher than that of mesoporous silica. The low adsorption capacity is reasonable.

Sorption thermodynamics of U(VI), Th(IV), and Eu(III) onto SiO_2–BDAH

The thermodynamic parameters (ΔH^0, ΔS^0, and ΔG^0) for U(VI), Th(IV), and Eu(III) sorption onto SiO_2–BDAH can be determined from the temperature dependence. The free energy

changes (ΔG^0) can be calculated from the following relationship [31, 32]:

$$\Delta G = -RT \ln K^0 \quad (10)$$

where R is the universal gas constant (8.3145 J mol^{-1} K^{-1}), T is the absolute temperature (K), and K^0 is the sorption equilibrium constant. K^0 is obtained by plotting lnK_d versus C_{eq} and extrapolating C_{eq} to zero at different temperatures (Fig. 8d–f). Its intercept with the vertical axis gives the value of lnK^0. The lnK^0 obtained from Fig. 8d–f at the three temperatures is listed in Table 4. Standard entropy changes (ΔS^0) are calculated using the following Eq. (11):

$$\left(\frac{\partial \Delta G^0}{\partial T}\right)_P = -\Delta S^0 \quad (11)$$

The average standard enthalpy change (ΔH^0) is then calculated from the following relationship (12):

$$\Delta H^0 = \Delta G^0 + T\Delta S^0 \quad (12)$$

The thermodynamic data calculated from Eqs. (10)–(12) listed in Table 4. The positive enthalpy change (ΔH^0) indicates the sorption of U(VI), Th(IV) and Eu(III) onto SiO_2–BDAH is endothermic, and a high temperature is good for the sorption process. The ΔH^0 of U(VI) and Eu(III) sorption increases when the temperature increases but is the reverse for Th(IV) sorption. The Th(IV) sorption process has probably a different mechanism for its high charge than U(VI) and Eu(III). The positive ΔS^0 for U(VI), Th(IV) and Eu(III) sorption onto SiO_2–BDAH varies with temperature change, and a higher temperature results to a higher ΔS^0 except for the Th(IV) sorption. A weak effect of temperature to Th(IV) sorption onto SiO_2–BDAH was observed for ΔS^0 and ΔH^0 that varied slightly. The negative ΔG^0 for U(VI), Th(IV) and Eu(III) sorption onto SiO_2–BDAH suggests that the sorption is spontaneous. ΔG^0 becomes more negative with increased temperature, which indicates that more efficient sorption occurs at high temperatures.

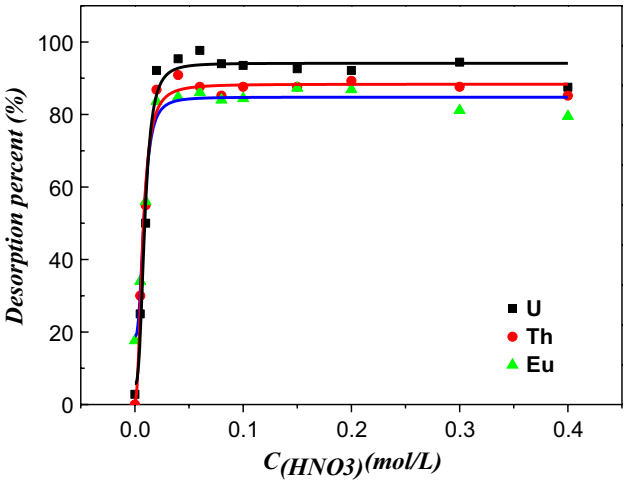

Fig. 9 Effect of the eluent concentration on the desorption of U(VI), Th(IV), and Eu(III) onto SiO_2–BDAH. C(UO_2^{2+})$_0$ = 2.0 × 10^{-4} mol/L, m/V = 2.5 g/L, C(Na^+) = 0.1 mol/L, pH = 5.0 ± 0.1, T = 25 ± 2 °C, t = 2 h; C(Th^{4+})$_0$ = 2.0 × 10^{-4} mol/L, m/V = 2.5 g/L, C(Na^+) = 0.1 mol/L, pH = 3.0 ± 0.1, T = 25 ± 2 °C, t = 2 h; C(Eu^{3+})$_0$ = 2.0 × 10^{-4} mol/L, m/V = 2.5 g/L, C(Na^+) = 0.1 mol/L, pH = 5.0 ± 0.1, T = 25 ± 2 °C, t = 2 h

Desorption Performance Study

The effect of eluent concentration on U(VI), Th(IV), and Eu(III) desorption from SiO_2–BDAH on was investigated. As shown in Fig. 9, diluted HNO_3 is very effective regenerate for organic sorbents, on account of carboxyl on the sorbent would be responsible for the sorption of U(VI), Th(IV), and Eu(III) while the process is very sensitive to pH. The 0.02 mol/L HNO_3 shows a better performance in the desorption of U(VI), Th(IV), and Eu(III), indicated that ionic exchange reaction is easy to happen between hydrogen ion and U(VI), Th(IV), and Eu(III) [38]. Desorption is a fast process and finished in 2 h.

Table 4 Thermodynamic functions for the sorption of U(VI), Th(IV), and Eu(III) onto SiO_2–BDAH at different temperatures

Metal ions	Temperature (K)	lnK^0 (mL/g)	R^2	ΔG (kJ/mol)	ΔS (J/mol K)	ΔH (kJ/mol)
UO_2^{2+}	338	6.68	0.924	− 18.78	165.28	37.12
	318	5.85	0.8807	− 15.47	109.82	19.47
	298	5.81	0.9677	− 14.39	54.36	1.82
Th^{4+}	338	7.86	0.9724	− 22.08	134.67	23.44
	318	7.34	0.9641	− 19.34	145.79	26.97
	298	6.56	0.9365	− 16.26	156.91	30.51
Eu^{3+}	318	7.52	0.9431	− 19.89	255.86	61.47
	308	6.77	0.8127	− 17.33	178.04	37.5
	298	6.59	0.9657	− 16.33	100.22	13.54

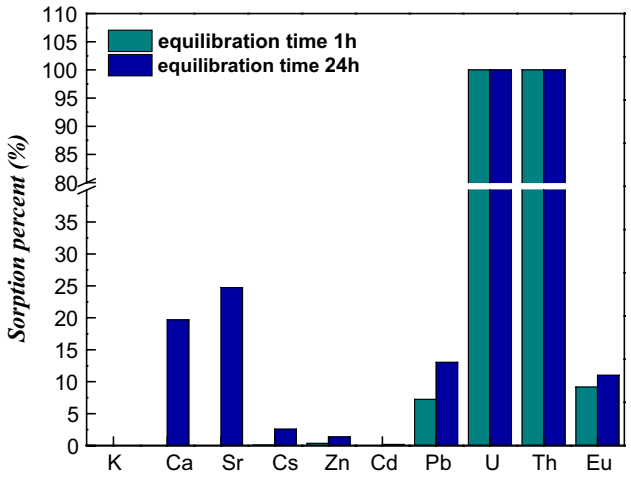

Fig. 10 Selectivity of U(VI), Th(IV), and Eu(III) onto SiO_2–BDAH. [M] = 1×10^{-5} mol/L, m/V = 5 g/L, pH = 3.0 ± 0.1, T = 25 ± 2 °C

Sorption Selectivity

Based on the presence of a variety of metal ions in radioactive wastewater, it is necessary for sorbents to have high selectivity for U(VI), Th(IV), and Eu(III). As shown in Fig. 10, SiO_2–BDAH exhibits good adsorption selectivity for U(VI), and Th(IV) when shaking time is 1 or 24 h, with the presence of multiple ions. Eu(III) experiences weaker sorption, but still stronger than all the foreign ions. Under 1 h contact time, SiO_2–BDAH shows high selectivity except for Pb(II). After 24 h, its selectivity weakens through the long-term contact by making adsorption to Ca(II), Sr(II), Cs(I) and Zn(II) but the sorption capacities for U(VI) and Th(IV) are still the highest of all. According to Fig. 10, SiO_2–BDAH can extract U(VI), and Th(IV) almost completely and Eu(III) partially from radioactive wastewater in weak acidic condition through short-time contact.

The adsorbents from previous work are compared with SiO_2–BDAH in Table 5 by their sorption capacities (q_{max}) and their corresponding experimental pH values as a vital parameter. It is obvious that SiO_2–BDAH has a larger sorption capacity for U(VI) and Th(IV) than unmodified SiO_2 at lower pH, while a lower sorption capacity for Eu(III) than other modified SiO_2 adsorbents. Overall, SiO_2–BDAH is an excellent sorbent, which could be used to remove U(VI), Th(IV), and Eu(III) together through short-time contact from aqueous solutions.

Conclusion

Our work aimed at exploring more sorbent, which is cheap, involves simple synthesis, and has good sorption characteristic. From our results, SiO_2–BDAH has the same structure and sorption behavior for U(VI), Th(IV), and Eu(III) as SiO_2–DGAH. The equilibrium sorption time for U(VI) and Th(IV) onto SiO_2–BDAH is 2 and 3 h, respectively and that for Eu(III) is 10 h. The sorption percentage of U(VI), Th(IV), and Eu(III) onto SiO_2–BDAH is lower for SiO_2–DGAH at low pH but is the reverse at high pH. The sorption process of U(VI), Th(IV) and Eu(III) can be described by the Langmuir model, and the sorption capacity of U(VI), Th(IV) and Eu(III) is 5.10×10^{-5}, 5.06×10^{-5}, and 3.44×10^{-5} mol/L at 298 K, respectively. The enthalpy and entropy changes are all positive, and the free energy change is negative. Hence, the sorption reaction is spontaneous and

Table 5 Comparison of the adsorption capacity of U(VI), Th(IV), and Eu(III) with other adsorbents reported in the literatures

Ion	Sorbent	pH	Adsorption capacity (mg/g)	Refs.
U(VI)	SiO_2–BDAH	2.8 ± 0.1	12.14	This work
	Sulfonated silica	1.5–2.2	73.8	[39]
	Unmodified SiO_2	4.24	1.25	[40]
	Modified activated carbon	5.0	20	[41]
	Unmodified silica gel	5.5	16.66	[42]
Th(IV)	SiO_2–BDAH	2.1 ± 0.1	11.84	This work
	Modified benzophenone	6.0–6.5	1.1	[43]
	Sulfated-b-CD@NAA	2.5	12.77	[44]
	Perlite	4.5	36.2	[45]
Eu(III)	SiO_2–BDAH	3.9 ± 0.1	5.23	This work
	DGSR-I	3 M HNO_3	10.4 ± 0.1	[26]
	SBA/EnSA	4	15	[46]
	Si–DGAH	3	8.2	[14]
	Modified silica nanoparticles	5.5	7.69	[7]
	DGA-SBA	1 M HNO_3	57.6	[17]

is advantageous when temperature increase. U(VI), Th(IV), and Eu(III) can be desorbed from SiO_2–DGAH easily using 0.02 mol/L nitric acid. SiO_2–BDAH is an effective sorbent, which extracts U(VI), and Th(IV) completely and quickly in the presence of multiple ions.

Acknowledgements Financial support from the National Science Foundation of China (Grants 21571088, 21876073).

References

1. Fan B, Meng Y, Liu J, Xiao J, Chen S, Cao J, Wu Y, Liu C (2002) Commercial experiment on bacteria heap leaching of uranium ore from caotaobei mining area in ganzhou uranium mine. Uranium Min Metall 21:67–73
2. Guo GL, Luo MB, Xu JJ, Wang TX, Hua R, Sun YZ (2009) Separation and continuous determination of the light rare earth elements and thorium in Baotou Iron Ore by a micro-column. J Radioanal Nucl Chem 281:647–651
3. Yuan LY, Bai ZQ, Zhao R, Liu YL, Li ZJ, Chu SQ, Zheng LR, Zhang J, Zhao YL, Chai ZF, Shi WQ (2014) Introduction of bifunctional groups into mesoporous silica for enhancing uptake of thorium(IV) from aqueous solution. ACS Appl Mater Interfaces 6:4786–4796
4. Whitty-Léveillé L, Reynier N, Larivière D (2018) Rapid and selective leaching of actinides and rare earth elements from rare earth-bearing minerals and ores. Hydrometallurgy 177:187–196
5. Zornitza T, Antoine K, Inna T (2006) Investigation of radioactive lead, uranium, and thorium in environmental waters by extraction chromatography resins. Int J Environ Anal Chem 86:653–661
6. Wang YL, Zhu L, Guo BL, Chen SW, Wu WS (2014) Mesoporous silica SBA-15 functionalized with phosphonate derivatives for uranium uptake. New J Chem 38:3853–3861
7. Shiri-Yekta Z, Yaftian MR, Nilchi A (2013) Silica nanoparticles modified with a Schiff base ligand: an efficient adsorbent for Th(IV), U(VI) and Eu(III) ions. Korean J Chem Eng 30:1644–1651
8. Wan IW, Abd Ali LI, Sulaiman A, Sanagi MM, Aboul-Enein HY (2014) Application of solid-phase extraction for trace elements in environmental and biological samples: a review. Crit Rev Anal Chem 44:233–254
9. Sarafraz H, Minuchehr A, Alahyarizadeh G, Rahimi Z (2017) Synthesis of enhanced phosphonic functional groups mesoporous silica for uranium selective adsorption from aqueous solutions. Sci Rep 7:11675–11682
10. Yousefi SR, Ahmadi SJ, Shemirani F, Jamali MR, Salavati-Niasari M (2010) Simultaneous extraction and preconcentration of uranium and thorium in aqueous samples by new modified mesoporous silica prior to inductively coupled plasma optical emission spectrometry determination. Talanta 80:212–217
11. Kırkan B, Aycik GA (2016) Solid phase extraction using silica gel modified with azo-dyes derivative for preconcentration and separation of Th(IV) ions from aqueous solutions. J Radioanal Nucl Chem 308:81–91
12. Venkatesan KA, Sukumaran V, Antony MP, Rao PRV (2004) Extraction of uranium by amine, amide and benzamide grafted covalently on silica gel. J Radioanal Nucl Chem 260:443–450
13. Tian Y, Pin Y, Qu RJ, Wang CH, Zheng HG (2010) Removal of transition metal ions from aqueous solutions by adsorption using a novel hybrid material silica gel chemically modified by triethylene-tetramino-methylene-phosphonic acid. Chem Eng J 162:573–579
14. Suneesh AS, Syamala KV, Venkatesan KA, Antony MP, Rao PRV (2015) Diglycolamic acid modified silica gel for the separation of hazardous trivalent metal ions from aqueous solution. J Colloid Interface Sci 438:55–60
15. Zhang L, Zhai Y, Chang X, He Q, Huang XP, Hu Z (2009) Determination of trace metals in natural samples by ICP-OES after preconcentration on modified silica gel and on modified silica nanoparticles. Microchimi Acta 165:319–327
16. Qu R, Niu Y, Sun C, Ji C, Wang C, Cheng GX (2006) Syntheses, characterization, and adsorption properties for metal ions of silica-gel functionalized by ester- and amino-terminated dendrimer-like polyamidoamine polymer. Microporous Mesoporous Mater 97:58–65
17. Shusterman JA, Mason HE, Bowers J, Bruchet A, Uribe EC, Kersting AB, Nitsche H (2015) Development and testing of diglycolamide functionalized mesoporous silica for sorption of trivalent actinides and lanthanides. ACS Appl Mater Interfaces 7:20591–20599
18. Kursunlu AN, Guler E, Dumrul H, Kocyigit O, Gubbuk IH (2009) Chemical modification of silica gel with synthesized new Schiff base derivatives and sorption studies of cobalt (II) and nickel (II). Appl Surf Sci 255:8798–8803
19. Moftakhar MK, Dousti Z, Yaftian MR, Ghorbanloo M (2016) Investigation of heavy metal ions adsorption behavior of silica-supported Schiff base ligands. Desalin Water Treat 57:1–13
20. Wang Q, Gao W, Liu Y, Yuan J, Xu Z (2014) Simultaneous adsorption of Cu(II) and SO_4^{2-}, ions by a novel silica gel functionalized with a ditopiczwitterionic Schiff base ligand. Chem Eng J 250:55–65
21. Pereira AS, Ferreira G, Caetano L, Martines MA, Padilha PM (2010) Preconcentration and determination of Cu(II) in a fresh water sample using modified silica gel as a solid-phase extraction adsorbent. J Hazard Mater 175:399–403
22. Filho NLD, Gushikem Y, Polito WL, Moreira J, Ehirim EO (1995) Sorption and preconcentration of metal ions in ethanol solution with a silica gel surface chemically modified with benzimidazole. Talanta 42:1625–1630
23. Sasaki Y, Sugo Y, Suzuki S, Tachimori S (2001) The Novel Extractants, Diglycolamides, for the Extraction of Lanthanides and Actinides in HNO_3-n-dodecane System. Solvent Extr Ion Exch 19:91–103
24. Edwards HGM, Hickmott E, Hughes MA (1997) Vibrational spectroscopic studies of potential amidic extractants for lanthanides and actinides in nuclear waste treatment. Spectrochim Acta A 53:43–53
25. Prasanta K, Mohapatra Seraj A, Ansari Mudassir I, Jurriaan H, Willem V (2014) First example of diglycolamide-grafted resins: synthesis, characterization, and actinide uptake studies. RSC Adv 4:10412–10419
26. Ansari S, Mohapatra P, Iqbal M, Huskens J, Verboom W (2014) Sorption of americium(III) and europium(III) from, nitric acid solutions by a novel diglycolamide-grafted, silica-based resins: part 2. Sorption isotherms, column and radiolytic stability studies. Radiochim Acta 102:903–910
27. Hopkins PD, Mastren T, Florek J, Copping R, Brugh M, John KD, Nortier MF, Birnbaum ER, Kleitz F, Fassbender ME (2018) Synthesis and radiometric evaluation of diglycolamide functionalized mesoporous silica for the chromatographic separation of actinides Th, Pa and U. Dalton Trans 47:5189–5195
28. Serhan U, Savaş P, Gökhan C, Tümer F (2013) Solid phase extraction of Pb(II), Cu(II), Cd(II) and Cr(III) with syringe technique using novel silica-supported bis (diazoimine) ligands. Chem Eng J 220:420–430

29. Guo Z, Xu J, Shi K, Tang Y, Wu W, Tao Z (2009) Eu(III) adsorption/desorption on Na-bentonite: experimental and modeling studies. Colloid Surface A 339:126–133
30. Kriaa A, Hamdi N, Srasra E (2008) Surface properties and modeling potentiometric titration of aqueous illite suspensions. Surf Eng Appl Electrochem 44:217–229
31. Qian LJ, Hu PZ, Jiang ZJ, Geng YX, Wu WS (2010) Effect of pH, fulvic acid and temperature on the sorption of uranyl on ZrP_2O_7. Sci China Chem 53:1429–1437
32. Qian LJ, Zhao HuP, Geng Y, Wu W (2010) Effect of pH, fulvic acid and temperature on the sorption of uranyl on ZrP_2O_7. J Radioanal Nucl Chem 283:653–660
33. Qian LJ, Cui WW, Liu YR, Hu PZ (2016) Sorption of Eu(III) on $Th_4(PO_4)_4P_2O_7$: effects of pH, complexing anions and fulvic acid. J Radioanal Nucl Chem 308:165–172
34. Kogermann K, Veski P, Rantanen J, Naelapää K (2011) X-ray powder diffractometry in combination with principal component analysis-a tool for monitoring solid state changes. Eur J Pharm Sci 43:278–289
35. Ishmuratov GY, Yakovleva MP, Mingaleeva GR, Muslukho RR, Vyrypaev EM, Galkin EG, Ivanov SP, Tolstikov AG (2009) Synthesis of macrolides with N-containing (azine or hydrazide) groups. Chem Nat Compd 45(4):465–469
36. Liu Y, Li L, Liu SW, Xie CX, Yu ST (2016) Synthesis of silanized magnetic Ru/Fe_3O_4@SiO_2 nanospheres and its high selectivity to prepare Cis-pinane. RSC Adv 6:81310–81317
37. Juère E, Florek J, Larivière D, Kim K, Kleitz F (2016) Support effects in rare earth element separation using diglycolamide-functionalized mesoporous silica. New J Chem 40:4325–4334
38. Duan GJ, Zhong QQ, Bi L, Yang L, Liu TH, Shi XN, Wu WS (2017) The poly(acrylonitr ule-co-acrylic acid)-graft-β-cyclodextrin hydrogel for thorium(IV) adsorption. Polymers 9:201
39. Abd EMMO, Soliman AGSA, Abd EAAM, Eldesouky EM (2018) Uranium extraction by sulfonated mesoporous silica derived from blast furnace slag. J Nucl Mater 509:295–304
40. Zhang HX, Wen CX, Tao ZY, Wu WS (2011) Effects of nitrate, fulvate, phosphate, phthalate, salicylate and catechol on the sorption of uranyl onto SiO_2: a comparative study. J Radioanal Nucl Chem 287(1):13–20
41. Mahmoud ME, Khalifa MA, El Wakeel YM, Header MS, Abdel-Fattah TM (2017) Engineered nano-magnetic iron oxide-urea-activated carbon nanolayer sorbent for potential removal of uranium (VI) from aqueous solution. J Nucl Mater 487:13–22
42. Sadeghi S, Sheikhzadeh E (2008) Solid phase extraction using silica gel functionalized with Sulfasalazine for preconcentration of uranium(VI) ions from water samples. Microchim Acta 163(3–4):313–320
43. Preetha CR, Gladis JM, Rao TP (2002) Solid phase extractive preconcentration of thorium onto 5,7-dichloroquinoline-8-ol modified benzophenone. Talanta 58(4):701–709
44. Qi CX, Liu HJ, Deng SX, Yang AH, Li ZD (2018) A modeling study by response surface methodology (RSM) on Th(IV) adsorption optimization using a sulfated β-cyclodextrin inclusion complex. Res Chem Intermed 44(4):1–23
45. Talip Z, Eral M, Hiçsönmez Ü (2009) Adsorption of thorium from z aqueous solutions by perlite. J Environ Radioact 100(2):139–143
46. Dolatyaria L, Yaftiana MR, Rostamnia S (2015) Adsorption characteristics of Eu(III) and Th(IV) ions onto modified mesoporous silica SBA-15 materials. J Taiwan Inst Chem Eng 60:174–184